

Chaos and complexity in a cardiac pacemaker model with incommensurate fractional-order dynamics: Empirical validation and cardiovascular implications

Haneche Nabil and Hamaizia Tayeb

Citation: Chin. Phys. B, 2026, 35 (**7**): 078702. DOI: 10.1088/1674-1056/ae0b3c
http://cpb.iphy.ac.cn; http://iopscience.iop.org/cpb

What follows is a list of articles you may be interested in

Dynamical behavior analysis for small-world scale-free neural networks

Jieyu Lu(鲁婕妤), Jiapeng Ouyang(欧阳佳鹏), Xue Zhao(赵雪), and Minglin Ma(马铭磷)
Chin. Phys. B, 2026, 35 (**6**): 068708. DOI: 10.1088/1674-1056/ae3609

Conduction failure in axonal signal propagation: Effects of I_h in a Hodgkin-Huxley cable model

Rong Hu(胡榕) and Yong Xie(谢勇)
Chin. Phys. B, 2026, 35 (**6**): 068706. DOI: 10.1088/1674-1056/ae5c7a

Anti-interference ability of spiking neuron-astrocyte networks in working memory

Lin Li(李琳), Bingyi Mo(莫冰毅), Shanshan Cheng(程姗姗), Zhouchao Wei(魏周超), Ming Yi(易鸣), and Lulu Lu(鹿露露)
Chin. Phys. B, 2026, 35 (**6**): 068703. DOI: 10.1088/1674-1056/ae4e8c

A visually meaningful medical image encryption scheme based on image steganography and memristive Hopfield neural networks

Wei Yao(姚卫), Xiangyun Huang(黄翔云), Jianhua Xiao(肖捡花), Fei Yu(余飞), and Yichuang Sun(孙义闯)
Chin. Phys. B, 2026, 35 (**6**): 068702. DOI: 10.1088/1674-1056/ae395d

Frequency-tunable spiking dynamics of Chua corsage memristors

Qijian Wu(吴奇键), Peipei Jin(靳培培), Xiameng Wu(吴夏萌), Meiyuan Gu(顾梅园), Wei Zhou(周玮), Yujiao Dong(董玉姣), Yan Liang(梁燕), and Long Chen(陈龙)
Chin. Phys. B, 2026, 35 (**4**): 048703. DOI: 10.1088/1674-1056/ae3c95

Chaos and complexity in a cardiac pacemaker model with incommensurate fractional-order dynamics: Empirical validation and cardiovascular implications

Haneche Nabil[1,†] and Hamaizia Tayeb[2]

[1] *Applied Mathematics and Modeling Laboratory, Department of Mathematics, Faculty of Exact Sciences, University of Mentouri Brothers, Constantine, Algeria*

[2] *Mathematical Modeling and Simulation Laboratory, Department of Mathematics, Faculty of Exact Sciences, University of Mentouri Brothers, Constantine, Algeria*

(Received 5 August 2025; revised manuscript received 7 September 2025; accepted manuscript online 25 September 2025)

The dynamics of heart rhythms plays a pivotal role in physiological health, where chaotic behavior is often associated with pathological cardiac states. In this work, we investigate a fractional-order model of cardiac pacemaker dynamics using incommensurate derivatives to capture the complex memory effects and non-local interactions inherent in biological systems. We demonstrate that slight variations in the fractional orders induce rich dynamics, including chaos and coexisting attractors, signifying transitions between normal and dysfunctional rhythms. Crucially, our model exhibits wider chaotic regions than classical integer-order counterparts when the incommensurate derivatives are perturbed. Furthermore, we reveal pronounced multistability, where distinct chaotic attractors coexist under identical parameters, reflecting the system's capacity for abrupt transitions between physiological and pathological states. These findings advance the mechanistic understanding of rhythm disorders and highlight the critical role of fractional calculus in modeling cardiac dynamics.

Keywords: cardiac pacemaker model, incommensurate fractional-order rhythm dynamics, chaos, bistability

PACS: 87.19.Hh, 05.45.–a, 02.30.Hq, 05.45.Pq

DOI: 10.1088/1674-1056/ae0b3c **CSTR:** 32038.14.CPB.ae0b3c

1. Introduction

Natural systems exhibit rhythmic patterns that range from regular to disordered, corresponding to either healthy or pathological states in biomedical contexts. The cardiovascular system's rhythm dynamics have been extensively researched due to the heart's vital physiological role.[1] This hollow muscular organ features four chambers (two atria and two ventricles) and a conduction system comprising self-excitatory components: the sinoatrial (SA) node, atrioventricular (AV) node, and His–Purkinje network.[2,3] Under normal conditions, the SA node initiates electrical impulses that propagate through the atria, AV node, and His–Purkinje system to myocardial cells, establishing it as the natural pacemaker. Cardiac dynamics are analyzed through mathematical modeling and time-series approaches. Van der Pol and Van der Mark[4] pioneered nonlinear oscillator models for heartbeat dynamics, with subsequent modifications simulating natural pacemaker action potentials. dos Santos *et al.*[5] extended these methods through coupled oscillators representing dual-pacemaker interactions, while Gois and Savi[6] modeled electrocardiogram (ECG) patterns using three delay-coupled oscillators. Several studies indicate chaotic characteristics in certain arrhythmias. Glass *et al.*[7] identified period-doubling bifurcations and chaotic dynamics in stimulated cardiac cell aggregates. ECG signal analysis reveals complex dynamics without requiring prior knowledge of the underlying system.[8] Other studies demonstrate both nonlinear deterministic and stochastic features in canine fibrillation, chaotic attributes in human ECGs via Poincaré maps and entropy metrics, and the combined influence of instabilities and environmental fluctuations on rhythm patterns.[9–12]

Fractional differential equations, characterized by non-integer-order derivatives, extend classical calculus to model systems with memory and non-local interactions.[13,14] The defining attributes of fractional-order derivatives include non-locality and memory, which enable the incorporation of system history and distributed spatial effects, contrasting sharply with the local properties of integer-order derivatives. This memory property allows fractional calculus to more realistically model hereditary processes in natural systems compared to traditional integer-order operators.[15,16] The resurgence of interest in fractional calculus stems from its superior capacity to simultaneously accommodate nonlinearity, historical dependencies, and distributed parameters, offering enhanced accuracy in modeling several real-world complex behaviors.[17,18]

In biological systems, fractional differential equations have been increasingly adapted to incorporate long-range temporal memory effects prevalent in physiological processes.[19]

†Corresponding author. E-mail: nabil.haneche@doc.umc.edu.dz

© 2026 Chinese Physical Society and IOP Publishing Ltd. All rights, including for text and data mining, AI training, and similar technologies, are reserved.

This capability is especially valuable in systems exhibiting metastable states with high electrical polarization. In cardiac electrophysiology, the sinoatrial node's pacemaking function exhibits history-dependent behaviors, where action potential generation is influenced by prior membrane potential states and ion channel activity.[20] The integration of fractional operator memory properties into cardiac pacemaker models significantly improves the representation of rhythm-generating dynamics by accounting for historical electrical states and recovery processes.

Recent studies have demonstrated promising applications of fractional calculus in cardiac modeling. Templos-Hernandez *et al.*[21] incorporated fractional dynamics into a nonlinear model of three coupled oscillators, finding that normal cardiac rhythms correspond to fractional orders near 1. Bellout *et al.*[22] introduced a fractional-order discrete map for cardiac action potential duration (APD) incorporating a "fixed memory length" to enhance physiological realism. Belmiloudi[23] developed a "memory bidomain system" using a time-fractional-order nonlinear reaction-diffusion model to represent cardiac memory. Additional research includes fractional-order Van der Pol oscillator models for the SA node[24] and fractional-order controllers for pacemakers.[25,26]

However, a critical analysis of existing literature reveals several important limitations that this work aims to address. Most current fractional-order cardiac models utilize commensurate fractional orders, which restrict the dynamic representation of the heart's multi-scale conduction system. Furthermore, many studies vary either fractional orders or physiological parameters in isolation, failing to explore their synergistic effects on transitions between healthy periodic rhythms and pathological chaotic states. There is also a notable scarcity of quantitative complexity analysis specifically adapted for fractional-order systems to objectively characterize these dynamical transitions. Finally, the phenomenon of bistability and attractor coexistence, which is crucial for understanding sudden cardiac state shifts, remains largely unexplored within the framework of incommensurate fractional-order cardiac models.

Motivated by these research gaps, our work introduces a novel incommensurate fractional-order model of the cardiac pacemaker. The main contributions are as follows.

(i) Development of an incommensurate fractional-order differential system that extends classical pacemaker models, capturing complex memory-dependent electrophysiological properties through a derived numerical solution.

(ii) Comprehensive investigation of heart rhythm transitions through simultaneous variation of incommensurate fractional orders and physiological parameters, revealing bistable states and attractor coexistence phenomena.

(iii) Implementation of the C_0 complexity algorithm to quantitatively characterize transitions between ordered and chaotic pacemaker dynamics, establishing a novel metric for pathological rhythm identification.

The remainder of this paper is organized as follows. Section 2 presents the cardiac pacemaker model. Section 3 derives the numerical solution for its incommensurate fractional-order counterpart. Section 4 investigates dynamic transitions under parameter variations. Section 5 applies complexity analysis using the C_0 algorithm. Section 6 explores bistability and attractor coexistence. Finally, Section 7 summarizes the main findings and suggests future research directions.

2. Description of the model

The mathematical modeling of heartbeat dynamics originated with the coupled nonlinear oscillators proposed by Van der Pol and Van der Mark.[4] The Van der Pol equation has since become a cornerstone for modeling cardiac rhythms due to its ability to replicate essential biological features, including limit cycles, synchronization phenomena, and chaotic behavior.[27,28] A key physiological advantage is its capacity to adapt the intrinsic frequency to external driving signals without amplitude distortion.

The modified Van der Pol oscillator proposed by Grudziński and Żebrowski[27] provides a physiologically grounded representation of cardiac pacemaker dynamics

$$\ddot{x}+\alpha(x-v_1)(x-v_2)\dot{x}+\frac{x(x+d)(x+e)}{ed}=F(t), \qquad (1)$$

where α governs pulse morphology (modulating stimulus timing), v_1 and v_2 create asymmetric damping, e controls atrial/ventricular contraction periods, d emerges from cubic forcing substitution, and $F(t)$ represents external stimuli. By converting this equation into state-space form, we obtain

$$\begin{cases} \dot{x}_1 = x_2, \\ \dot{x}_2 = F(t)-\alpha(x_1-v_1)(x_1-v_2)x_2-\dfrac{x_1(x_1+d)(x_1+e)}{ed}. \end{cases} \qquad (2)$$

Figure 1 outlines the cardiac pacemaker framework, showcasing essential conduction elements and their physiological interactions.

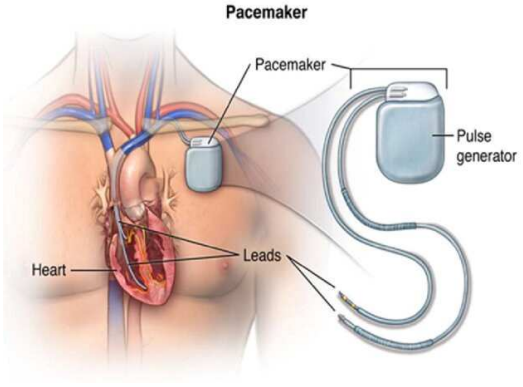


Fig. 1. Schematic diagram of the cardiac pacemaker model.[29]

Several definitions of fractional-order derivatives exist, including the Riemann–Liouville, Caputo, and Grünwald–Letnikov definitions. These formulations have been widely employed in fractional calculus. Our objective is to extend the above framework using incommensurate fractional-order derivatives to capture the memory effects and non-local interactions inherent in cardiac tissue.

The classical integer-order formulation of cardiac rhythm models has been extensively documented to generate diverse dynamical regimes, including periodic, quasi-periodic, and chaotic oscillations. In the present work, we fundamentally extend this paradigm by introducing incommensurate fractional-order derivatives into the governing equations. Our investigation focuses on how variations in these fractional orders reconfigure the system's dynamical landscape, particularly by examining wider chaotic regions under parameter variations and bifurcations associated with arrhythmic transitions. Moreover, it demonstrates a variety of coexisting attractors that represent pathological conditions.

3. Numerical method for solving fractional-order differential equations

Three principal definitions dominate fractional calculus: Riemann–Liouville, Caputo, and Grünwald–Letnikov. For broad function classes with zero initial conditions and lower terminal $a = 0$, these formulations become mathematically equivalent.[30]

Definition 1[31] The Riemann–Liouville fractional derivative of a continuous function $f : [a, +\infty) \to \mathbb{R}$ of order θ $(m-1 < \theta < m, m \in \mathbb{N})$ is defined as

$$ {}^{RL}_{a}\mathcal{D}^{\theta}_{t} f(t) = \frac{\mathrm{d}^m}{\mathrm{d}t^m}\left[\frac{1}{\Gamma(m-\theta)}\int_a^t \frac{f(\tau)}{(t-\tau)^{\theta-m+1}}\,\mathrm{d}\tau\right], \quad (3) $$

where $\Gamma(\cdot)$ denotes the Euler gamma function that generalizes the factorial to real and complex numbers.

While mathematically rigorous, this definition poses interpretation challenges for physical systems. Notably, fractional derivatives of constants are non-zero, complicating the specification of initial conditions.

Definition 2[32] The Caputo fractional derivative of a continuous function $f : [a, +\infty) \to \mathbb{R}$ of order θ $(m-1 < \theta < m, m \in \mathbb{N})$ is defined as

$$ {}^{C}_{a}\mathcal{D}^{\theta}_{t} f(t) = \frac{1}{\Gamma(m-\theta)}\int_a^t \frac{f^{(m)}(\tau)}{(t-\tau)^{\theta-m+1}}\,\mathrm{d}\tau. \quad (4) $$

The Caputo fractional derivative definition offers a key advantage: it retains standard initial conditions identical to those of integer-order systems, enhancing practical utility. However, its dependence on integral operators and gamma functions complicates direct numerical implementation.[30]

3.1. Computational approach

Direct numerical implementation of Caputo's definition is hindered by its integral form and dependence on gamma functions. For efficient discretization, the Grünwald–Letnikov fractional derivative definition is employed.

Definition 3[33] The Grünwald–Letnikov fractional derivative of a continuous function $f : [a, +\infty) \to \mathbb{R}$ of order θ is defined as

$$ {}^{GL}_{a}\mathcal{D}^{\theta}_{t} f(t) = \lim_{h\to 0} h^{-\theta} \sum_{j=0}^{\left\lfloor \frac{t-a}{h} \right\rfloor} (-1)^j \binom{\theta}{j} f(t-jh), \quad (5) $$

where $\lfloor\cdot\rfloor$ denotes the floor function, a specifies the memory length, and the binomial coefficients are

$$ \binom{\lambda}{0} = 1, \quad \binom{\lambda}{j} = \frac{\lambda(\lambda-1)\cdots(\lambda-j+1)}{j!}, \quad j \geq 1. \quad (6) $$

Numerical solutions of fractional systems necessitate handling memory effects and retaining historical states. Two predominant approximation methods exist: frequency-domain methods and time-domain methods.[34,35] Frequency-domain methods are efficient, but they may compromise the accuracy of transient responses and increase computational costs. Time-domain methods implement history-dependent schemes, such as the Adams–Bashforth–Moulton predictor-corrector algorithm.[36] For cardiac rhythm modeling, we prioritize time-domain methods despite their higher computational costs. Their superior reliability in chaotic regime detection is essential for identifying pathological transitions in fractional-order pacemaker dynamics.

3.2. Numerical implementation for cardiac rhythm model

We implement the Grünwald–Letnikov derivative (Definition 3) with the short memory principle to solve our fractional-order cardiac pacemaker Eq. (1). This approach substantially reduces memory requirements while maintaining numerical reliability. The technique leverages the observation that, for large t, contributions from initial conditions $(t = 0)$ become negligible in cardiac rhythm simulations.

Applying the short memory principle to our fractional-order cardiac model yields[30,37]

$$ \begin{aligned} \mathcal{D}^{\theta_1}_{t_k} x_1 &\approx \lim_{h\to 0} \frac{1}{h^{\theta_1}} \sum_{j=0}^{\lfloor N(t)\rfloor} (-1)^j \binom{\theta_1}{j} x_1(t_{k-j}) \\ &\approx h^{-\theta_1} \sum_{j=0}^{\lfloor N(t)\rfloor} c_j^{(\theta_1)} x_1(t_{k-j}), \\ \mathcal{D}^{\theta_2}_{t_k} x_2 &\approx \lim_{h\to 0} \frac{1}{h^{\theta_2}} \sum_{j=0}^{\lfloor N(t)\rfloor} (-1)^j \binom{\theta_2}{j} x_2(t_{k-j}) \\ &\approx h^{-\theta_2} \sum_{j=0}^{\lfloor N(t)\rfloor} c_j^{(\theta_2)} x_2(t_{k-j}), \end{aligned} \quad (7) $$

where h is the integration step size, $t_k = kh$, $N(t) = \min\left(\frac{t_k - L}{h}, \frac{L}{h}\right)$ represents the memory length truncation, and $c_j^{(\theta_i)}$ $(i = 1, 2)$ are coefficients that can be computed recursively as

$$c_0^{(\theta_i)} = 1, \quad c_j^{(\theta_i)} = \left(1 - \frac{1+\theta_i}{j}\right) c_{j-1}^{(\theta_i)}. \tag{8}$$

By incorporating the memory characteristics of the cardiac pacemaker system defined by Eq. (2), the model can be expressed as a fractional differential equation of the following form:

$$\begin{cases} {}_0^{GL}\mathcal{D}_t^{\theta_1} x_1(t) = x_2, \\ {}_0^{GL}\mathcal{D}_t^{\theta_2} x_2(t) = F(t) - \alpha(x_1 - v_1)(x_1 - v_2)x_2 \\ \qquad\qquad - \dfrac{x_1(x_1 + d)(x_1 + e)}{ed}, \end{cases} \tag{9}$$

where θ_1 and θ_2 are arbitrary non-integer orders.

The discretization of the system is performed using the explicit approximation of fractional derivatives given in Eq. (7), resulting in the following discretized form of the system in Eq. (9)

$$\begin{aligned} x_1(t_k) &= [x_2(t_{k-1})]\, h^{\theta_1} - \sum_{j=1}^{N-1} c_j^{(\theta_1)} x_1(t_{k-j}), \\ x_2(t_k) &= \left[F(t_k) - \alpha(x_1(t_k) - v_1)(x_1(t_k) - v_2)x_2(t_{k-1}) \right. \\ &\quad \left. - \frac{x_1(t_k)(x_1(t_k) + d)(x_1(t_k) + e)}{ed}\right] h^{\theta_2} \\ &\quad - \sum_{j=1}^{N-1} c_j^{(\theta_2)} x_2(t_{k-j}), \end{aligned} \tag{10}$$

where $k = 1, 2, \ldots, N$, and $c_j^{(\theta_i)}$ represent the binomial coefficients that can be determined according to Eq. (8).

All numerical simulations were performed using MATLAB R2021a with integration step $h = 1 \times 10^{-3}$ and total simulation time $T_{\text{sim}} = 500$, in which the initial 1000 iterations were discarded to eliminate transients. Phase portraits and bifurcation diagrams were generated by systematically varying the incommensurate fractional orders (θ_1, θ_2) and pacemaker parameters (α, v_1, v_2, e, d). The initial conditions were selected as $(x_1(0), x_2(0)) = (-0.1, 0.025)$, consistent with the equivalence of fractional derivative definitions under these conditions.

4. Dynamics of the heart pacemaker

In this section, the dynamic behaviors of the cardiac pacemaker model (9) are analyzed according to slight variations in the system parameters and fractional orders, $\theta_i \in (0, 1]$, $i = 1, 2$. New results are established, including the instability of the system with incommensurate orders θ_i, bifurcations, maximum Lyapunov exponent (MLE), complexity analysis, and coexisting attractors. Parameters established by Grudziński and Żebrowski for modeling normal natural pacemaker activity were initially implemented.[27] The fixed parameter values used are $\alpha = 0.5$, $v_1 = 0.97$, $v_2 = -1$, $d = 3$, $e = 6$, and $F(t) = E\sin(\omega t)$. Here, E and ω represent the amplitude and frequency of the external cosinusoidal excitation, respectively. In the simulation, we take the constants as $E = 2.5$ and $\omega = 1.9$.

4.1. Dynamics with θ_i varying

Fix $\theta_2 = 0.96$ and let the incommensurate order θ_1 vary from 0.5 to 1 with a step size of $\Delta\theta_1 = 0.001$. The bifurcation diagram obtained by plotting the local maxima of the coordinate x_2 is shown in Fig. 1(a). As can be observed, system (9) exhibits stable oscillations when the incommensurate order θ_1 ranges between $0.5 \le \theta_1 \le 0.783$. However, as θ_1 exceeds 0.783, the first period-doubling bifurcation occurs, resulting in a period-2 cycle. As θ_1 increases further, the period-2 cycle loses its stability, and system (9) gradually develops chaos through a high-periodicity sequence of cycles. In this case, the route to chaos is a period-doubling bifurcation, and system (9) displays chaotic behavior at $\theta_1 = 0.933$.

In a deterministic dynamical system, chaotic behavior is determined by the existence of a positive Lyapunov exponent. This paper uses a numerical method based on the memory principle detailed in Refs. [38–40] to compute the maximum Lyapunov exponent of a fractional-order system discretized according to the Grünwald–Letnikov derivative definition. The result of the MLE simulation with respect to the incommensurate order θ_1 is shown in Fig. 1(b). From the MLE spectrum shown in Fig. 1(b), it can be seen that the MLE is strictly positive in the range $\theta_1 \in [0.933, 1]$, except for some periodic zones near $\theta_1 = 0.938$, $\theta_1 = 0.953$, and $\theta_1 = 0.997$, which implies chaotic dynamics in this parameter range with the appearance of certain periodic orbits.

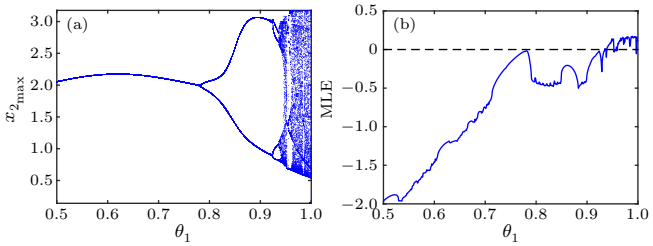


Fig. 2. Dynamical analysis of the cardiac pacemaker model (9): (a) bifurcation diagram with respect to θ_1; (b) MLE spectrum with respect to θ_1.

To analyze the impact of the incommensurate order θ_2 on the dynamics of the cardiac pacemaker model (9), we fix $\theta_1 = 0.985$ and vary the incommensurate order θ_2 from 0.4 to 1 with a step size of $\Delta\theta_2 = 0.001$. The bifurcation diagram obtained by plotting the local maxima of the coordinate x_2 is

shown in Fig. 3(a), while the corresponding MLE spectrum is depicted in Fig. 3(b).

One can see that changes in the incommensurate order θ_2 significantly impact the system's dynamics, resulting in stable and unstable states. When θ_2 is in the range of $[0.5, 0.58]$, stable oscillations occur, followed by the first period-doubling bifurcation of the system (9). At $\theta_2 = 0.776$, the system loses its stability and gradually develops chaos through a high-periodicity sequence of cycles. Similarly, in this case, the route to chaos is a period-doubling bifurcation, in which the chaotic zone shifts to the right with increasing incommensurate order, except for the appearance of a periodic zone near $\theta_2 = 0.961$. The MLE spectrum shown in Fig. 2(b) strongly validates the previous observations regarding the periodic and chaotic states.

For visualizing the chaotic response, phase diagrams and state trajectories of system (9) with different values of incommensurate orders are illustrated in Fig. 4.

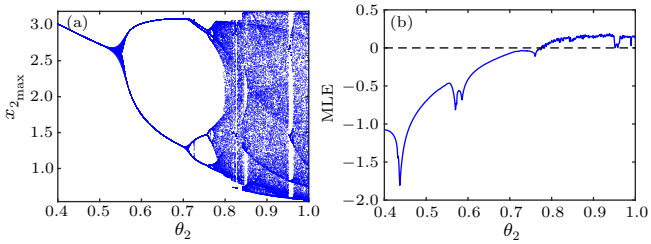


Fig. 3. Dynamical analysis of the cardiac pacemaker model (9): (a) bifurcation diagram with respect to θ_2; (b) MLE spectrum with respect to θ_2.

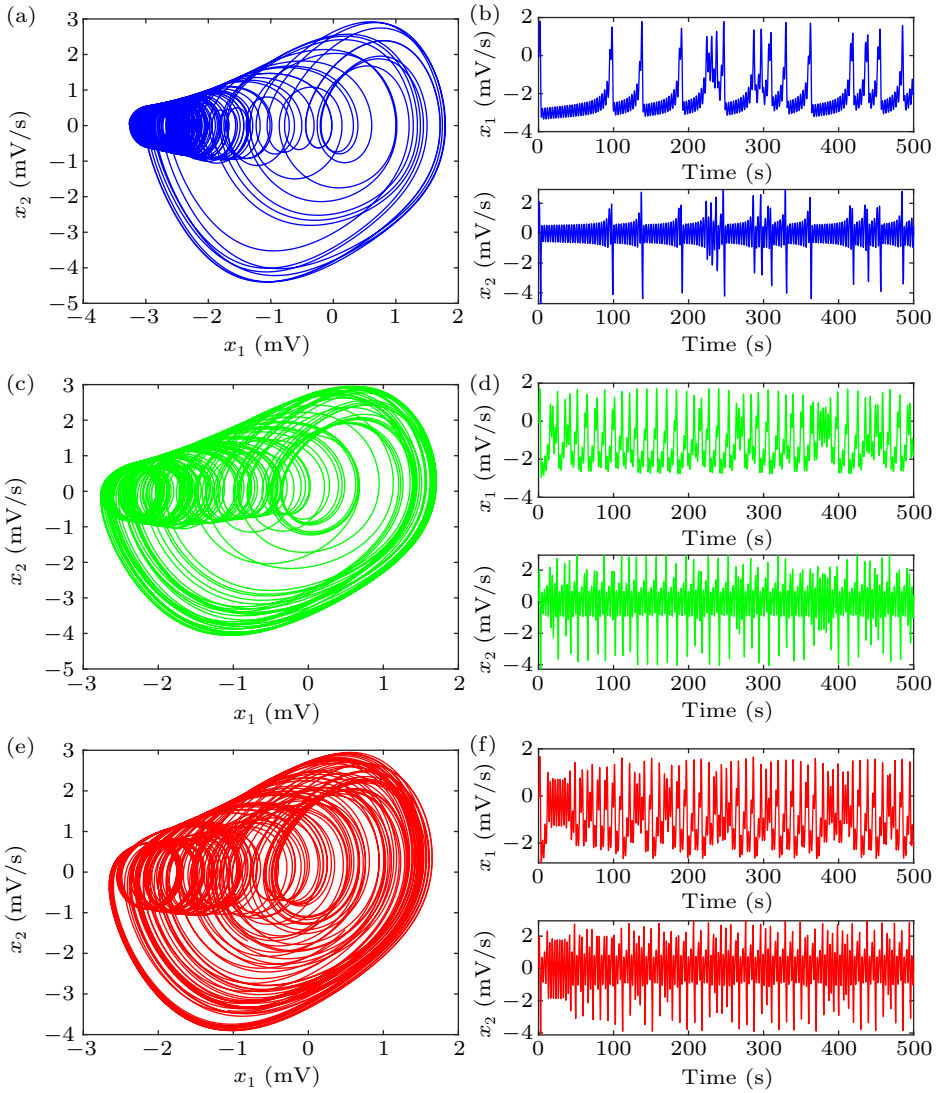


Fig. 4. Phase diagrams and state trajectories of the cardiac pacemaker model (9): (a)–(b) for $(\theta_1, \theta_2) = (0.985, 0.96)$; (c)–(d) for $(\theta_1, \theta_2) = (0.985, 0.98)$; (e)–(f) for $(\theta_1, \theta_2) = (0.965, 0.975)$.

For medical implications, chaotic dynamics emerging in the fractional-order cardiac pacemaker model under incommensurate orders signify critical pathological states. This represents sick sinus syndrome, where discordance between depolarization (θ_1-order) and repolarization (θ_2-order) dynamics generates unstable sinoatrial node firing, causing dangerous pauses and tachycardias. Such chaos models the transition to lethal fibrillations (atrial/ventricular), where spatiotemporal heterogeneity promotes reentrant wavelets and rotor formation, compromising cardiac output and increasing the risk of

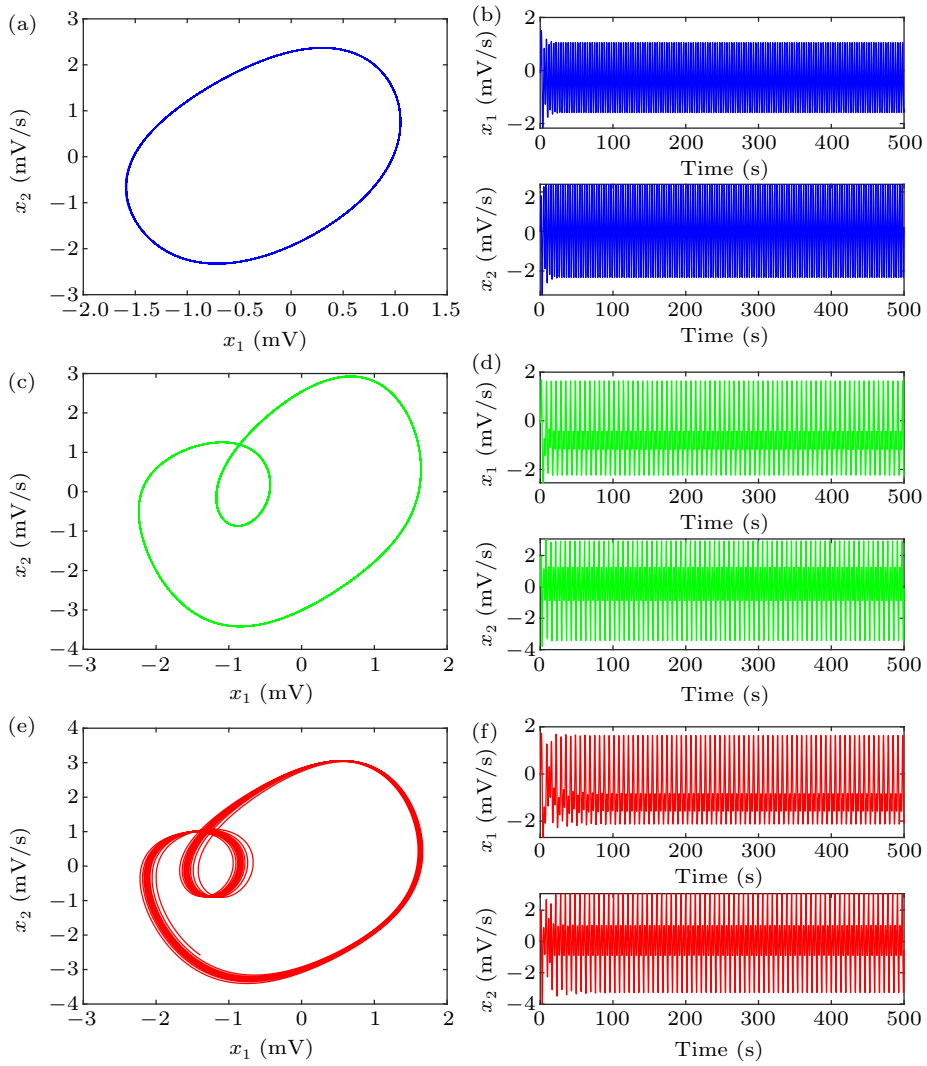


Fig. 5. Phase diagrams and state trajectories of the cardiac pacemaker model (9): (a)–(b) for $(\theta_1,\theta_2)=(0.845,0.869)$; (c)–(d) for $(\theta_1,\theta_2)=(0.894,0.876)$; (e)–(f) for $(\theta_1,\theta_2)=(0.931,0.877)$.

stroke or sudden death. The incommensurability mimics ion channelopathies and electrical remodeling associated with myocardial infarction or heart failure, where pathological memory effects create vulnerable substrates for torsades de pointes and ectopy-triggered arrhythmias. Clinically, this chaos corresponds to the loss of pacemaker periodicity, extreme sensitivity to stimuli, and unpredictable restitution. This condition is a hallmark of electrophysiological instability and requires urgent intervention to prevent hemodynamic complications.

For visualizing the periodic response, phase diagrams and state trajectories of system (9) with different values of incommensurate orders are illustrated in Fig. 5. Both kinds of responses can be depicted by considering different initial conditions. The chaotic response can be observed in Fig. 6(a), which shows the Poincaré section for $(x_1(0),x_2(0))=(-0.1,0.025)$. Furthermore, Fig. 6(b) shows the basin of attraction of the cardiac pacemaker model (9) for the above set of parameters and different initial conditions. It illustrates the coexistence of a period-1 attractor (black zone) and a chaotic attractor (red zone).

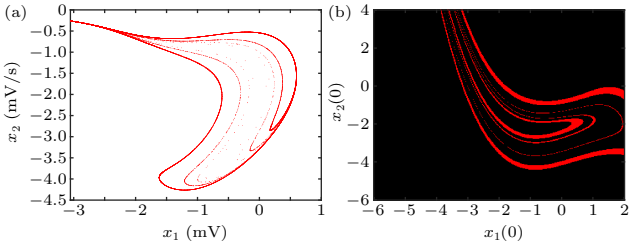


Fig. 6. Simulation results of the cardiac pacemaker model (9): (a) Poincaré section; (b) basin of attraction showing the coexistence of a period-1 attractor (black) and a chaotic attractor (red).

4.2. Dynamics with α varying

In the proposed cardiac pacemaker model, the control parameter α governs pulse morphology and modulates stimulus timing by scaling the nonlinear damping term $-\alpha(x_1-v_1)(x_1-v_2)x_2$. This parameter directly controls the stability and excitability of oscillations. Variations in α can induce transitions between quiescent states, limit cycles (regular pacing), and complex dynamics such as chaos, making it a primary candidate for bifurcation analysis.

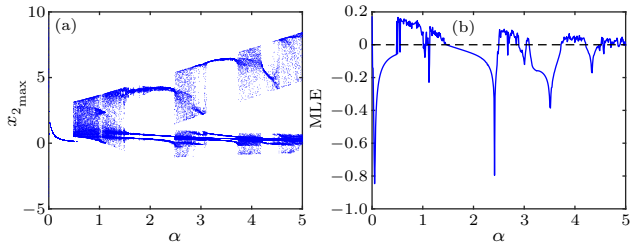


Fig. 7. Dynamical analysis of the cardiac pacemaker model (9): (a) bifurcation diagram with respect to α; (b) MLE spectrum with respect to α.

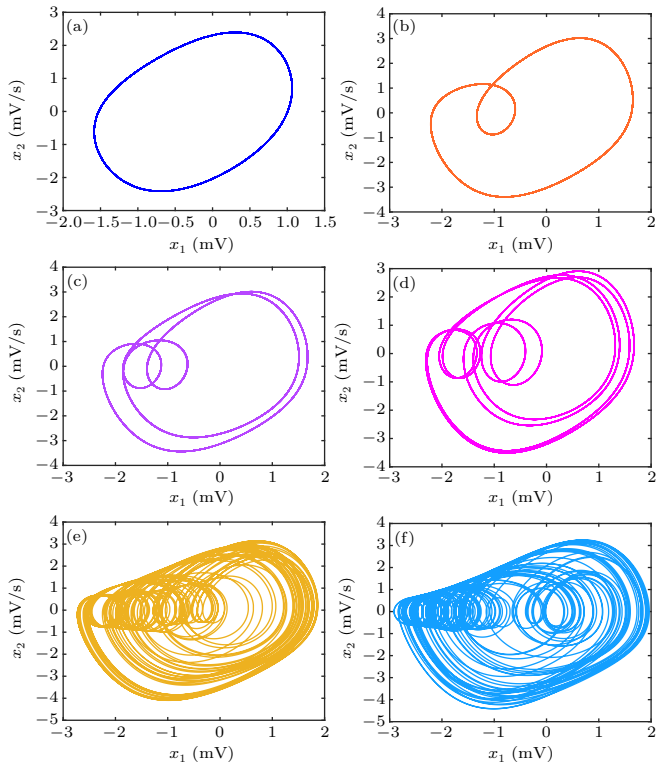


Fig. 8. Phase diagrams of the cardiac pacemaker model (9): (a) period-1 orbit for $\alpha = 0.262$; (b) period-2 orbit for $\alpha = 1.02$; (c) period-4 orbit for $\alpha = 2.189$; (d) period-8 orbit for $\alpha = 3.565$; (e) chaotic attractor for $\alpha = 4.729$; (f) chaotic attractor for $\alpha = 5$.

Fix the fractional orders as $(\theta_1, \theta_2) = (0.985, 0.98)$, and let the control parameter α vary in the range $[0,5]$ with a step size of $\Delta\alpha = 0.01$. The bifurcation diagram obtained by plotting the local maxima of the coordinate x_2 is shown in Fig. 7(a), while the MLE spectrum is depicted in Fig. 7(b). As can be seen, periodic and chaotic regions are observed. When the control parameter α ranges over $[0,0.47]\cup[0.97,1.14]\cup[1.47,2.49]\cup[2.86,3.02]\cup[3.09,3.71]\cup[4.19,4.56]$, system (9) exhibits stable dynamics, where the system is either periodic or converges to an equilibrium point, as validated by the negative MLE. However, in the remaining regions of the interval $[0,5]$, the MLE is strictly positive, indicating chaotic behavior.

To provide further clarification of the periodic and chaotic responses, phase diagrams of the pacemaker model (9) with different values of the control parameter α are shown in Fig. 8.

For medical implications, periodic behavior, typically observed for various values of α, represents the healthy and regular rhythm generation essential for normal cardiac function, where the sinoatrial node reliably produces synchronized electrical impulses. However, chaotic behavior induced by increasing α beyond critical thresholds may model pathological cardiac arrhythmias, such as ventricular fibrillation or chaotic atrial tachycardia, characterized by unpredictable and erratic electrical activity that severely compromises the heart's pumping efficiency, potentially leading to hemodynamic collapse or sudden cardiac death if uncorrected. This highlights the role of α as a critical parameter whose dysregulation, reflecting underlying physiological changes such as ischemia or electrolyte imbalance, can destabilize the pacemaker system from stable rhythm maintenance into life-threatening dynamical states, thus providing a theoretical framework for understanding arrhythmogenesis and potentially guiding antiarrhythmic drug development or pacing strategies aimed at restoring periodicity.

Gottwald and Melbourne[41] introduced a novel diagnostic method called the 0–1 test to identify chaotic behavior in deterministic dynamical systems. This study employs the 0–1 test to detect chaotic dynamics within experimental data. The technique is generally applicable to deterministic systems and offers the distinct advantage of bypassing phase-space reconstruction. For a given time series, the test generates a binary output (0 for regular or 1 for chaotic dynamics).[42] Given a temporal observable $x(j)$, the dimensionless coordinates in the (p,s)-plane are computed as

$$\begin{cases} p(n) = \sum_{j=1}^{n} x(j)\cos(jc), \\ s(n) = \sum_{j=1}^{n} x(j)\sin(jc), \end{cases} \tag{11}$$

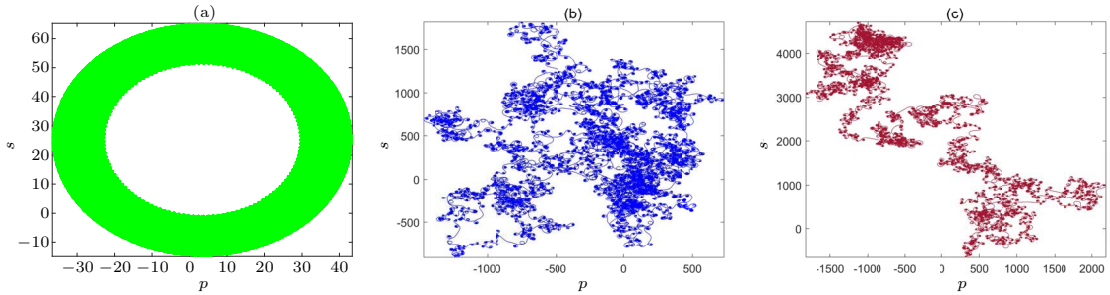


Fig. 9. Plots of the (p,s) trajectories of the 0–1 test: (a) for $\alpha = 0.262$; (b) for $\alpha = 4.729$; (c) for $\alpha = 5$.

where c denotes an arbitrary constant randomly selected from $(0,\pi)$, and $n = 500$ experimental data points are utilized for chaotic system analysis.

Figure 9 depicts the (p,s) trajectories of the 0–1 test, validating the previous results of periodic or chaotic responses in the proposed incommensurate pacemaker model.

5. Complexity analysis

While the maximum Lyapunov exponent can quantify the complexity of a chaotic system and provide qualitative insights into chaotic behavior, it lacks the quantitative precision required for practical applications. Thus, relying solely on this numerical tool is insufficient for accurate analysis. To address this limitation, we employ the C_0 algorithm to better evaluate the complexity of the cardiac pacemaker model. The C_0 complexity metric provides a robust numerical evaluation of chaotic sequences by measuring the energy contained in non-dominant spectral components associated with isolated irregularities.[43] In brief, we review the steps of the C_0 complexity algorithm.

For a discrete signal $x(n)$ of length N ($n = 0,1,\ldots,N-1$), the procedure is implemented as follows:

(i) Compute average spectral power: Calculate the mean squared magnitude of the discrete Fourier transform (DFT) coefficients $X(k)$

$$P_{\text{avg}} = \frac{1}{N}\sum_{k=0}^{N-1}|X(k)|^2. \tag{12}$$

(ii) Threshold DFT coefficients: Suppress coefficients below γP_{avg} (where $\gamma > 0$ is a selectivity parameter)

$$X_{\text{thr}}(k) = \begin{cases} X(k), & \text{if } |X(k)|^2 > \gamma P_{\text{avg}}, \\ 0, & \text{otherwise.} \end{cases} \tag{13}$$

(iii) Reconstruct periodic approximation: Synthesize the thresholded signal via the inverse DFT

$$x_{\text{per}}(n) = \frac{1}{N}\sum_{k=0}^{N-1} X_{\text{thr}}(k)\,\mathrm{e}^{\mathrm{j}2\pi kn/N}. \tag{14}$$

(iv) Compute complexity measure: Define C_0 as the normalized residual energy after removing periodic components[44]

$$C_0(\gamma,N) = \frac{\sum_{n=0}^{N-1}|x(n)-x_{\text{per}}(n)|^2}{\sum_{n=0}^{N-1}|x(n)|^2}. \tag{15}$$

This metric $C_0(\gamma,N)$ represents the relative energy attributable to non-periodic signal components, with higher values indicating greater irregularity.

For the numerical simulations, the incommensurate order θ_2 is fixed at 0.96, and the C_0 complexity of the incommensurate fractional-order cardiac pacemaker system (9) with varying θ_1 is calculated, as shown in Fig. 10(a). According to Fig. 10(a), the system exhibits higher complexity when it is chaotic. The C_0 complexity results agree well with the MLE spectrum. The system has higher complexity when the incommensurate order θ_1 exceeds 0.933.

Additionally, Fig. 10(b) shows the C_0 complexity with respect to the incommensurate order θ_2, while keeping θ_1 fixed at 0.985. As can be observed, periodic ranges correspond to lower complexity levels. Higher complexity levels are obtained in the chaotic regions of the incommensurate order. In particular, when θ_2 exceeds 0.776, the complexity of the proposed system increases rapidly. Thus, varying the incommensurate orders significantly impacts the dynamical behavior of system (9), and caution should be exercised when selecting the fractional orders to achieve the high complexity level required for practical applications. Similarly, the C_0 complexity of the cardiac pacemaker model (9) with varying control parameter α is shown in Fig. 10(c).

The 2D contour plots shown in Figs. 10(d)–10(f) demonstrate the complexity distribution according to the incommensurate orders (θ_1,θ_2) (Fig. 10(d)), (θ_1,α) (Fig. 10(e)), and (θ_2,α) (Fig. 10(f)). The regions with concentrated colors emphasize high complexity levels, indicating chaotic ranges for the system parameters.

High complexity in cardiac pacemaker models may generate chaotic dynamics, leading to unpredictable and irregular pacing outputs. This may disrupt stable heart rhythm regulation and potentially trigger dangerous arrhythmias, such as ventricular tachycardia or fibrillation. Ultimately, such chaotic behavior could compromise pacing performance and increase the risk of adverse cardiac events.

For a more in-depth analysis, a quantitative comparison is provided in this study. Figure 11 displays the MLE spectrum and C_0 complexity of system (9) alongside three other fractional-order non-autonomous chaotic systems: the biological system,[45] the Duffing double-well oscillator,[46] and the tabu learning single neuron (TLSN) model.[47] In this comparison, we set $\theta_1 = \theta_2 = \theta$. The results in Fig. 11(a) demonstrate that system (9) exhibits a broader chaotic region and a higher maximum Lyapunov exponent (reaching a peak value of 0.154) compared with the other systems. In particular, the proposed system shows more extensive chaotic characteristics than the neuron model, which displays only a narrow parameter range with a slightly positive Lyapunov exponent. Moreover, as illustrated in Fig. 11(b), the proposed system generates chaotic sequences with higher complexity, indicating greater unpredictability. Although the Duffing double-well oscillator also shows considerable complexity, it does not exceed that of the pacemaker model (9), which attains a peak complexity value of 0.405. This enhanced dynamical complexity suggests that the proposed system is well suited for real-world applications, such as secure information transmission. The key findings of this comparative analysis are summarized in Table 1.

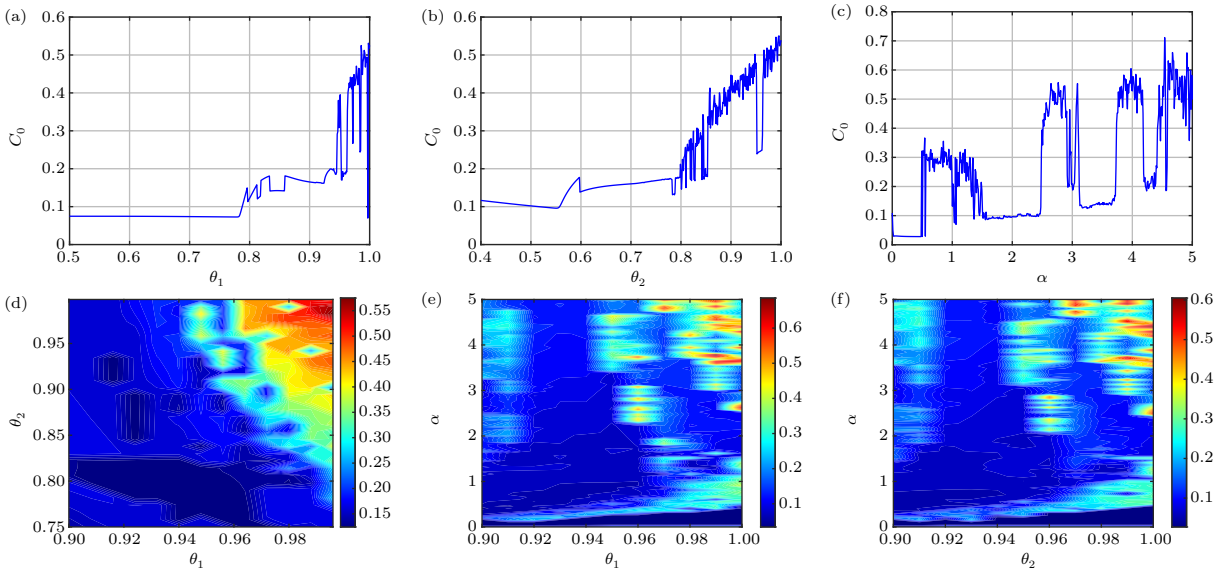


Fig. 10. C_0 complexity of the cardiac pacemaker model (9): (a) as a function of θ_1 with $\theta_2 = 0.96$; (b) as a function of θ_2 with $\theta_1 = 0.985$; (c) as a function of α with $(\theta_1, \theta_2) = (0.985, 0.98)$; (d) C_0-based chaos diagram with $\alpha = 0.5$ in the (θ_1, θ_2)-plane; (e) C_0-based chaos diagram with $\theta_2 = 0.96$ in the (θ_1, α)-plane; (f) C_0-based chaos diagram with $\theta_1 = 0.985$ in the (θ_2, α)-plane.

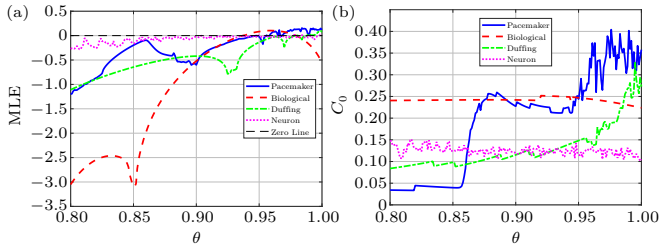


Fig. 11. MLE spectrum and C_0 complexity of different fractional-order non-autonomous chaotic systems: (a) comparison based on the MLE spectrum; (b) comparison based on C_0 complexity.

Table 1. Comparison of complexity between fractional-order non-autonomous chaotic systems.

Model	Chaotic range	MLE	C_0-based complexity
Proposed pacemaker model	$[0.956, 1]$	0.154	0.405
Biological system[45]	$[0.938, 0.978]$	0.103	0.329
Duffing oscillator[46]	$[0.976, 0.981] \cup [0.994, 1]$	0.075	0.251
TLSN neuron model[47]	$[0.994, 1]$	0.019	0.151

6. Bistability and coexistence attractors

Bistability in fractional-order chaotic systems describes the phenomenon where two distinct stable attractors coexist within the same parameter set. Unlike integer-order systems, the inherent memory properties of fractional derivatives significantly enrich the potential for such coexisting attractors, which can include combinations of chaotic attractors, periodic orbits, or fixed points. Crucially, the final state of the system (i.e., which attractor it settles into) depends sensitively on the initial conditions, exhibiting a strong dependence on the basin of attraction.[48,49] This coexistence arises from the complex interaction between the fractional order's ability to interpolate dynamics and the system's nonlinearity, often revealing hidden attractors not found in classical models. Analyzing this bistability is vital, as it reflects enhanced multistability and complexity, impacting control strategies and secure communication applications. Understanding the basins and bifurcations governing these coexisting states remains a key research challenge.

Bistability in fractional-order pacemaker models provides a framework for understanding why the heart can abruptly switch from normal rhythm to dangerous chaotic arrhythmias based on small triggers and physiological history, and why restoring normal rhythm can be challenging, reflecting the persistence of pathological attractors.

For demonstrating the bistability of fractional-order system (9), the bifurcation diagrams of two solutions are plotted in Fig. 12(a) by varying the incommensurate order θ_2 in the range $\theta_2 \in [0.4, 1]$ and fixing $\theta_1 = 0.985$ with two ICs: $(x_1(0), x_2(0)) = (-0.1, 0.025)$ for the blue points and $(x_1(0), x_2(0)) = (1, -1)$ for the red points. From Fig. 12(a), it can be observed that there are two coexisting solutions of system (9). This indicates that the system remains in different dynamical regimes according to the two initial conditions when $0.776 \leq \theta_2 \leq 1$, where system (9) can exhibit the coexistence of various types of attractors, such as periodic and chaotic attractors. For instance, the coexistence of periodic attractors appears for $\theta_2 = 0.628$ and $\theta_2 = 0.772$, as shown in Figs. 12(b) and 12(c), respectively. Meanwhile, Fig. 12(d) illustrates the coexistence of chaotic attractors with $\theta_2 = 0.947$.

From a medical point of view, the coexistence of a periodic attractor and a chaotic attractor in a cardiac pacemaker model reflects the heart's dual potential for stable rhythmic pacing and dangerous unpredictable electrical behavior. The periodic state represents a healthy regular heartbeat essential

for normal function, while the chaotic state corresponds to life-threatening arrhythmias such as fibrillation. This coexistence implies that even when the system appears stable and rhythmic, an underlying vulnerability may exist. A small disturbance can abruptly shift the system from a safe, predictable rhythm into the chaotic basin. This model highlights the intrinsic fragility of cardiac dynamics and explains the sudden onset of catastrophic arrhythmias despite apparent stability, emphasizing the critical importance of maintaining physiological conditions to avoid transitions into chaotic states.

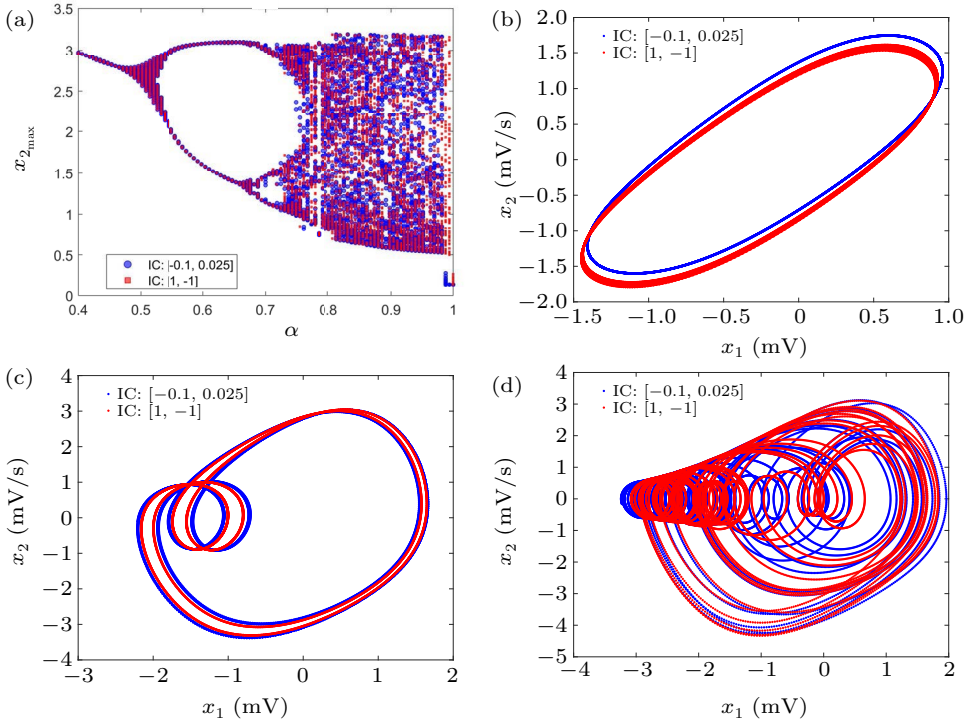


Fig. 12. Bistability of the cardiac pacemaker model (9): (a) bifurcation diagrams of the coexisting solutions of system (9) for $\theta_1 = 0.985$ with $(x_1(0), x_2(0)) = (-0.1, 0.025)$ for the blue points and $(x_1(0), x_2(0)) = (1, -1)$ for the red points; (b) coexisting period-1 orbit attractors with $\theta_2 = 0.628$; (c) coexisting period-4 orbit attractors with $\theta_2 = 0.772$; (d) coexisting chaotic attractors with $\theta_2 = 0.947$.

7. Conclusion and future works

Motivated by the inherent memory properties of biological systems, this study establishes a fractional-order cardiac pacemaker model with incommensurate derivatives to investigate its chaotic and periodic dynamics. By extending the classical integer-order framework through fractional calculus, we capture complex memory-dependent behaviors that are critical to cardiac rhythms. Through bifurcation diagrams, maximum Lyapunov exponents, phase plots, and complexity analysis, we demonstrate that variations in control parameters and fractional orders induce rich dynamical transitions: the system shifts between chaotic and periodic states, with non-integer orders acting as effective tools for suppressing pathological chaos and stabilizing periodic oscillations, providing a potential approach for pacemaker control. Furthermore, the quantification of complexity via the C_0 algorithm reveals how parameter sensitivity governs system unpredictability, while the identification of bistability and coexisting attractors (periodic and chaotic) underscores the model's dependence on initial conditions and fractional-order configurations. These findings highlight the dual role of bifurcation parameters and memory-rich fractional derivatives as tunable mechanisms for modulating cardiac dynamics, offering potential pathways for biomedical control strategies. However, our fractional model, derived from an integer-order framework rather than *ab initio* principles, may only partially approximate physiological dynamics. Crucially, formal stability analysis of the controlled system and synchronization of coupled pacemakers remain open challenges. Future work should develop efficient fractional-order controllers to exploit arbitrary non-integer orders for arrhythmia suppression, rigorously analyze stability bounds, and explore discrete equivalents for real-time implementation. This research bridges nonlinear dynamics and cardiac electrophysiology, advancing the potential of fractional calculus in designing resilient pacemaker systems through the principled control of memory, chaos, and multistability.

References

[1] Zhang J, Chatham J C and Young M E 2020 *Annu. Rev. Physiol.* **82** 79
[2] da Silva Lima G, Amorim Savi M and Moreira Bessa W 2024 *Sci. Rep.* **14** 23284
[3] Cheffer A, Savi M A, Pereira T L and de Paula A S 2021 *Appl. Math. Model.* **96** 152
[4] Van Der Pol B and Van Der Mark J 1928 *Lond. Edinb. Dubl. Phil. Mag.* **6** 763
[5] dos Santos A M, Lopes S R and Viana R R L 2004 *Phys. A* **338** 335

[6] Gois S R and Savi M A 2009 *Chaos Solitons Fractals* **41** 2553
[7] Glass L, Guevara M R, Shrier A and Perez R 1983 *Phys. D* **7** 89
[8] Henriques T, Ribeiro M, Teixeira A, Castro L, Antunes L and Costa-Santos C 2020 *Entropy* **22** 309
[9] Quiroz-Juárez M A, Vázquez-Medina R, Ryzhii E, Ryzhii M and Aragón J L 2017 *Commun. Nonlinear Sci. Numer. Simul.* **42** 370
[10] Wu G Q, Arzeno N M, Shen L L, Tang D K, Zheng D A, Zhao N Q, Eckberg D L and Poon C S 2009 *PloS One* **4** e4323
[11] Fonkou R F and Savi M A 2023 *Fractal Fract.* **7** 592
[12] Cheffer A and Savi M A 2020 *Biosystems* **196** 104177
[13] Vellappandi M and Lee S 2025 *Nonlinear Dyn.* **113** 12117
[14] Tarasov V E 2021 *Commun. Nonlinear Sci. Numer. Simul.* **102** 105947
[15] Fernández-Anaya G, Godínez F A, Valdés R, Quezada-Téllez R A and Polo-Labarrios M A 2025 *Fractal Fract.* **9** 264
[16] Barros L C, Lopes M M, Pedro F S, Esmi E, Santos J P C and Sánchez D E 2021 *Comput. Appl. Math.* **40** 72
[17] Haneche N and Hamaizia T 2024 *Phys. Scr.* **99** 115269
[18] Haneche N and Hamaizia T 2025 *Phys. Scr.* **100** 075253
[19] Kumar A and Kumar S 2022 *Chaos Solitons Fractals* **156** 111697
[20] Gratz D, Onal B, Dalic A and Hund T J 2018 *Front. Phys.* **6** 63
[21] Templos-Hernandez D J, Quezada-Tellez L A, Gonzalez-Hernandez B M, Rojas-Vite G, Pineda-Sanchez J E, Fernández-Anaya G and Rodriguez-Torres E E 2021 *Chaos Solitons Fractals* **147** 110942
[22] Bellout A, Bououden R, Houmor T and Berkal M 2025 *Gulf J. Math.* **19** 369
[23] Belmiloudi A 2021 *AIMS Math.* **6** 821
[24] Barbosa R S, Machado J T, Vinagre B M and Calderon A J 2007 *J. Vib. Control* **13** 1291
[25] Saleem O, Ahmed D and Iqbal J 2025 *Fractal Fract.* **9** 424
[26] Yürdem B, Aksu M F and Sağbaş M 2024 *Circuits Syst. Signal Process.* **43** 7423
[27] Grudziński K and Żebrowski J 2004 *Phys. A* **336** 153
[28] Savi M A 2005 *J. Braz. Soc. Mech. Sci. Eng.* **27** 157
[29] Al-Sharify N T, Rzaij D R, Nahi Z M and Al-Sharify Z T 2020 *IOP Conf. Ser.: Mater. Sci. Eng.* **870** 012020
[30] Petráš I 2011 *Fractional-Order Nonlinear Systems: Modeling, Analysis and Simulation* (Berlin, Heidelberg: Springer)
[31] Heymans N and Podlubny I 2006 *Rheol. Acta* **45** 765
[32] Murillo-Arcila M, Peris A and Vargas-Moreno Á 2025 *Fract. Calc. Appl. Anal.* **28** 1717
[33] Scherer R, Kalla S L, Tang Y and Huang J 2011 *Comput. Math. Appl.* **62** 902
[34] Adams D E and Allemang R J 2000 *Mech. Syst. Signal Process.* **14** 637
[35] Brandt A and Brincker R 2014 *Measurement* **58** 511
[36] Diethelm K, Ford N J and Freed A D 2002 *Nonlinear Dyn.* **29** 3
[37] Vinagre B M, Chen Y Q and Petráš I 2003 *J. Frankl. Inst.* **340** 349
[38] Danca M F and Fečkan M 2024 *Int. J. Bifurc. Chaos Appl. Sci. Eng.* **34** 2450156
[39] Danca M F and Kuznetsov N 2018 *Int. J. Bifurc. Chaos Appl. Sci. Eng.* **28** 1850067
[40] Li H, Shen Y, Han Y, Dong J and Li J 2023 *Chaos Solitons Fractals* **168** 113167
[41] Gottwald G A and Melbourne I 2009 *SIAM J. Appl. Dyn. Syst.* **8** 129
[42] Sun K H, Liu X and Zhu C X 2010 *Chin. Phys. B* **19** 110510
[43] Wang S, He S, Yousefpour A, Jahanshahi H, Repnik R and Perc M 2020 *Chaos Solitons Fractals* **131** 109521
[44] He S, Sun K and Wang H 2015 *Entropy* **17** 8299
[45] Hammouch Z and Mekkaoui T 2014 *Nonauton. Dyn. Syst.* **1** 61
[46] Zhang Y, Yue X, Du L, Wang L and Fang T 2016 *Shock Vib.* **2016** 6109062
[47] Bao H, Ding R, Chen B, Xu Q and Bao B 2023 *Chaos Solitons Fractals* **169** 113228
[48] Ye X and Wang X 2020 *Phys. Scr.* **95** 075212
[49] Han X, Mou J, Xiong L, Ma C, Liu T and Cao Y 2021 *Integration* **81** 43